PHYSICAL REVIEW B VOLUME 58, NUMBER 18 1 NOVEMBER 1998-II

Spin coherence excitation and rephasing with optically shelved atoms

B. S. Ham and M. S. Shahriar
Research Laboratory of Electronics, Massachusetts Institute of Technology, Cambridge, Massachusetts 02139

M. K. Kim
Physics Department, University of South Florida, Tampa, Florida 33620

P. R. Hemmer
Air Force Research Laboratory, Hanscom Air Force Base, Massachusetts 01731

(Received 17 August 1998)

We investigate the use of resonant optical Raman pulses to excite and rephase ground state spin coherences via the partial storage or shelving of atoms. Unlike direct-rf-excited spin echoes or off-resonant Raman echoes, the resonant Raman optical field efficiently excites and rephases the spin coherence using π and 2π pulses, respectively. In a crystal of Pr^{3+} doped Y_2SiO_5, we experimentally observe spin echo efficiency as high as 46% of the free induction decay signal. [S0163-1829(98)50142-7]

The excitation of spin coherent transients with lasers has many potential applications, for example, high resolution NMR spectroscopy of dilute spin samples,[1,2] resonant Raman optical memory,[3] high-resolution position sensing,[4] atom interferometry,[5] and quantum computing.[6] For these applications near maximal spin coherence amplitude is desired. To achieve such a large spin coherence amplitude using low intensity, cw lasers, resonant laser excitation is required.

Commonly used resonant optical techniques to excite spin coherences include coherent population trapping[7] (CPT), adiabatic passage[8] (AP), quantum beats[9] (QB), and coherent Raman beats[10] (CRB). Of these CPT has recently demonstrated the ability to create large amplitude spin coherences, capable of producing electromagnetically induced transparency[11] (EIT) in optically dense solids.[12] However, CPT is inherently an optical pumping process, and hence is inadequate when it is necessary to create a large amplitude spin coherence faster than the excited state decay rate. AP has been shown to rapidly produce EIT in vapors,[11] but requires optical pumping for state preparation in the case of spin sublevels with near equal thermal populations. QB can excite spin coherences more rapidly, but requires broadband laser pulses and has shown disappointing echo efficiency. CRB also has the potential to rapidly excite large amplitude coherence at low intensity, but has so far not demonstrated excitation of a large-amplitude spin coherence and has not been used to excite spin echoes.

In this paper we report fast optical excitation of large-amplitude spin coherence using relatively low intensity lasers. This technique relies on the shelving of atomic population in the excited state via a resonant Raman π pulse. We also show that efficient echo generation can be accomplished by applying a Raman 2π pulse. Although this technique has not been previously demonstrated using optical excitation, the π-2π echo model was predicted in QB,[13] and it was experimentally performed in microwave regime.[14] The echo efficiency in this earlier experiment was poor because it was based on a Raman-like system in which only one of the two electron-spin transitions was allowed.

To illustrate this technique in more detail, consider a three-level Λ-type system interacting with resonant Raman fields [see Fig. 1(a)], described in terms of dark ($|-\rangle$) and bright ($|+\rangle$) states [see Fig. 1(b)]. These are defined as

$$|-\rangle=[\Omega_2|1\rangle-\Omega_1|2\rangle]/\Omega, \tag{1a}$$

$$|+\rangle=[\Omega_1|1\rangle+\Omega_2|2\rangle]/\Omega, \tag{1b}$$

where $\Omega=\sqrt{\Omega_1^2+\Omega_2^2}$ and Ω_1,Ω_2 are the Rabi frequencies coupling states $|1\rangle$, $|2\rangle$, to state $|3\rangle$, respectively. In the coherent state basis [Fig. 1(b)], only the bright state $|+\rangle$ is coupled to the excited state $|3\rangle$ so that the system behaves like a two-level atom with an additional uncoupled state into which population can be trapped. The ground state spin coherence ρ_{12} can be expressed in this basis as

$$\mathrm{Re}(\rho_{12})=[\rho_{++}-\rho_{--}]/2, \tag{2}$$

where ρ_{++} and ρ_{--} are the ensemble averaged populations in the $|+\rangle$ and $|-\rangle$ states, respectively.

In the limit of long excited state lifetime (or large Rabi frequency), the dynamics are simply explained by Rabi flopping. In this case, the ground state spin coherence has sinusoidal time dependence as shown by the solid curve in Fig. 1(c). Here, equal Rabi frequencies have been assumed. As expected, maximum coherence (of $-1/4$) occurs for an optical pulse area of π, which corresponds to zero bright state population $\rho_{++}=0$. In the opposite limit of fast excited state lifetime (or small Rabi frequency), the spin coherence gradually increases to its maximum value (of $-1/2$) as the $|+\rangle$ state is emptied via CPT. This is shown by the dotted curve in Fig. 1(c). An intermediate case is plotted as the dashed curve which shows how the spin coherence evolves when the optical transition has a long excited state population decay time, but short coherence decay time. Here, the spin coherence initially evolves sinusoidally, but the oscillations rapidly damp out as the optical coherence dephases.

To understand how resonant Raman excitation can initiate rephasing (echoes), consider an atom left in only the $|-\rangle$ and

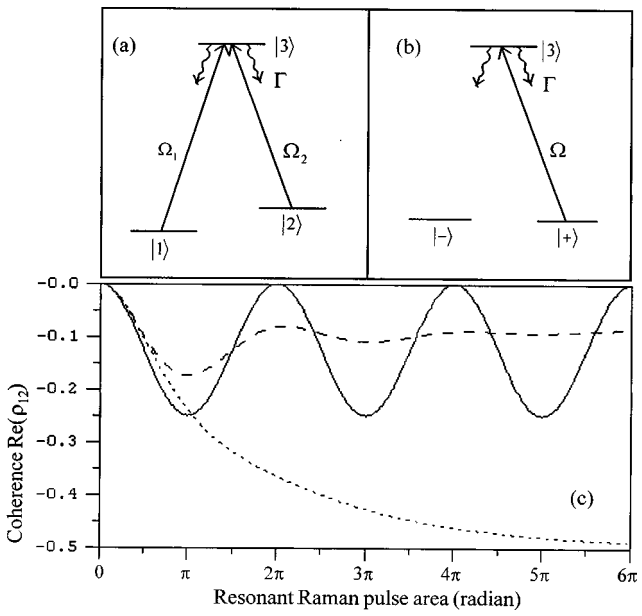

FIG. 1. Resonant Raman field interaction with a three-level system in (a) bare state basis and (b) coherent state basis. (c) Resonant Raman field excited spin coherence $\mathrm{Re}(\rho_{12})$ as a function of the Raman pulse area: (solid), $\Gamma=\gamma=0$; (dotted) $\Gamma=\gamma=3\Omega$; (dashed), $\Gamma=\Omega/30$ and $\gamma=\Omega$.

$|3\rangle$ states by the first pulse. Due to inhomogeneous broadening on the spin transition, the $|-\rangle$ state will acquire a $|+\rangle$ state contribution with time t according to

$$|\Psi_{\mathrm{ground}}(T)\rangle=[\cos(\delta t/2)|-\rangle+i\sin(\delta t/2)|+\rangle], \quad (3)$$

where δ is the detuning from two-photon (Raman) resonance for an atom away from the center of the inhomogeneously broadened transition. If at time $t=T$ a second resonant Raman pulse is applied, the $|+\rangle$ and $|3\rangle$ state contributions are exchanged by Rabi flopping. After an optical 2π pulse, the $|+\rangle$ state amplitude is returned to its original value, except for a π phase shift. This gives a new ground state contribution,

$$|\Psi'_{\mathrm{ground}}(T)\rangle=[\cos(\delta T/2)|-\rangle-i\sin(\delta T/2)|+\rangle]. \quad (4)$$

It is easy to show that this state evolves to a pure $|-\rangle$ state at time $t=2T$ that is independent of δ, thereby producing an efficient spin echo. Finally, the excited state $|3\rangle$ will also experience dephasing between pulses, especially in the presence of optical inhomogeneous broadening. However, this will not be rephased by the optical 2π pulse. Thus, even if the second pulse area is not exactly 2π, the excited state contribution will not adversely affect the spin echo.

To experimentally observe resonant optical Raman excited spin echoes, we chose a crystal of Y_2SiO_5 doped with Pr^{3+} ions. This material was chosen because the Pr ions have a relatively long optical and spin coherence lifetimes. The optical T_1 and T_2 are 111 and 164 μs, respectively, at 1.6 K.[15] The ground state spin lifetimes are on the order of 100 s for T_1 and 500 μs for T_2at 5 K.[3] For site 1, the optical oscillator strength of the $^3H_4\rightarrow{}^1D_2$ transition at 605.9 nm is relatively large for rare earth doped crystals, giving an absorption coefficient as large as 10 cm^{-1}.[16] The relevant energy sublevels of Pr^{3+} are shown in Fig. 2. The Raman resonant laser fields are ω_1 and ω_2. The field at ω_R is used to repump atoms that would otherwise accumulate in the state labeled $|0\rangle$. For efficient detection of ground state spin coherence, a probe beam at ω_P is used. This probe beam is red detuned by $\Delta=1$ MHz from the beam ω_2 and is Bragg matched to diffract light from the ground state coherence grating created by the (noncolinear) beams ω_1 and ω_2, which intersect at an angle of about 50 mrad. The diffracted light ω_D is then a sensitive measure of the amplitude of ground state coherence owing to enhanced nondegenerate four-wave mixing.[17] The four applied laser fields are derived from a single frequency stabilized dye laser using acousto-optic modulators (AOM), driven by frequency synthesizers as described elsewhere.[3] The use of AOM's makes laser jitters correlated so that laser difference frequencies are stable typically down to sub-kHz. To generate pulses, rf powers to the acousto-optic modulators are controlled by rf switches, driven by pulse generators (SRS DG 535). Typical pulse sequences begin with a 3 ms repump beam pulse, followed immediately by the first resonant Raman pulse. The second resonant Raman pulse is applied with a variable delay of time T from the first pulse. The first pulse width is 8 μs, and the second pulse width is 16 μs. The probe pulse has a width of 10 μs, and its delay time is scanned from just before the end of the repump pulse (-10 μs delay) to beyond the echo location in steps of 1 μs. The repetition rate of the entire pulse sequence is 50 Hz. To average out laser jitter effects, thirty diffracted signals are captured by a Boxcar averager (SRS 250) using a gate width of 5 μs positioned on top of the probe pulse. All laser beams are circularly polarized with a quarter wave plate, and focused into the sample by a 20 cm focal length lens. The beam diameters ($1/e$ in intensity) are $\sim$100 μm in the crystal. The size of the crystal is $3\times6\times4$ (mm) with its optical B axis along the 4 mm direction. The crystal temperature is kept at 5 K and the laser propagation direction is almost parallel to the crystal B axis.

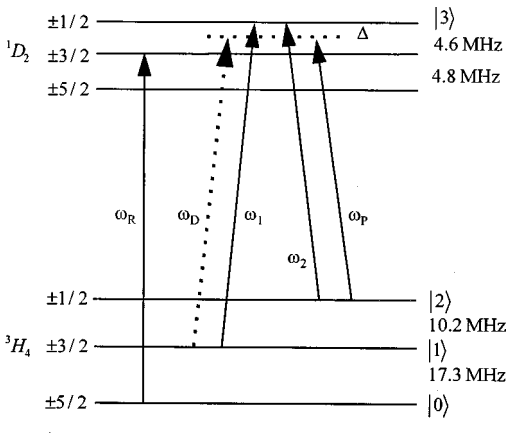

FIG. 2. Energy level diagram of $Pr^{3+}:Y_2SiO_5$.

Figure 3(a) illustrates the typical experimental resonant Raman pulse sequence. As mentioned above, each resonant Raman pulse is composed of both ω_1 and ω_2,and the second pulse is twice as wide as the first pulse. Figure 3(b) shows the experimental spin free induction decay (FID) and echo signals, as detected by monitoring the diffracted beam ω_D. The signal is strong enough to be detected by a photodiode instead of a photomultiplier. The pulse separation T is cho-

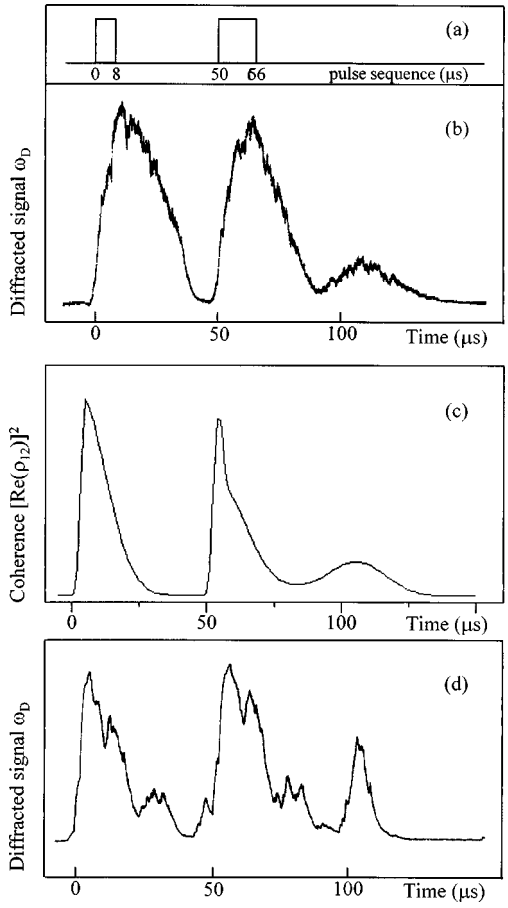

FIG. 3. Resonant Raman pulse excited spin echo at 5 K. (a) Resonant Raman pulse sequence. (b) Observed echo signals. The powers of ω_R, ω_1, ω_2, and ω_P are 9, 21, 1.5, and 2.8 mW, respectively. (c) Theoretical echo signal intensities for $\Gamma=\Omega/10$ and $\gamma=\Omega$. (d) Observed echo signals when the laser powers in (b) are increased by a factor of ~2, and beam diameters in the crystal are enlarged by a factor of ~1.5.

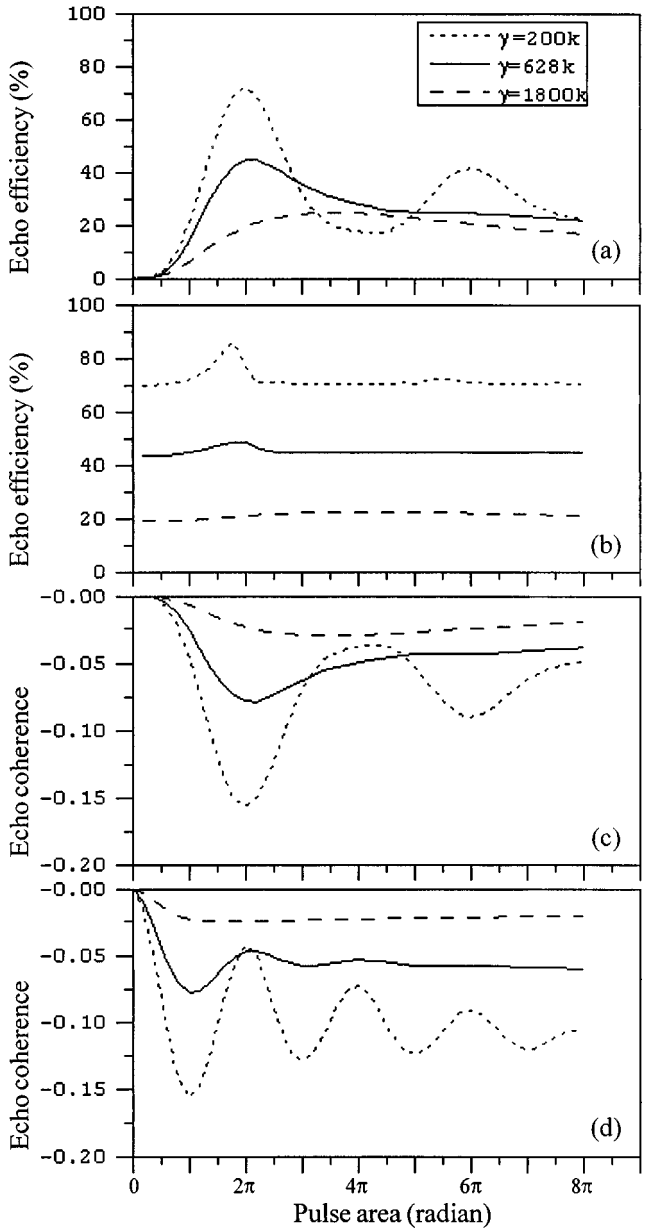

FIG. 4. Numerical calculation of resonant Raman pulse excited spin echo efficiencies and amplitudes vs the Raman pulse area. Curves in (a) show echo efficiencies for fixed first pulse are of π. Curves in (b) show echo efficiencies for fixed second pulse area of 2π. Plots in (c) and (d) show absolute echo amplitude corresponding to plots in (a) and (b), respectively. $\Omega=6.28\times10^5$ radian and $\Gamma=2\times10^4$ radian.

sen to be 1/10 of the spin T_2, and close to the optical population lifetime T_1. As shown in Fig. 3(b), the spin echo efficiency is 21% in intensity, which translates to 46% in amplitude. We found that the echo amplitude is not very sensitive to the width of either Raman pulse in the range of 5 μs–20 μs. From this, we suspect that the laser jitter is greater than the optical Rabi frequency (to be discussed in Fig. 4). The absolute power of the generated signal ω_D is ~0.1 mW which is ~4% of the input probe power. The noise in the FID and echo signals comes from both laser intensity and frequency jitter. The broader than expected FID signal width is attributed primarily to the probe pulse width of 10 μs.

Figure 3(c) shows the theoretical diffracted beam intensity ($\propto[\mathrm{Re}(\rho_{12})]^2$) as a function of time using parameters that correspond approximately to the experiment. This calculation assumes a closed three-level system with equal initial ground state populations. The excited state population decay rate Γ is chosen to be 10 kHz which is close to the actual lifetime at 5 K, and the optical coherence decay rate γ is chosen to be 100 kHz which is close to the measured decoherence rate due to the laser jitter. For simplicity, the spin decay rates are set to zero. The spin inhomogeneous width is chosen to be 15 kHz which is close to the measured value, and is assumed to have a Gaussian line shape. The optical Rabi frequency in the experiment is not known exactly as mentioned above, but assumed to be the same as the laser jitter (100 kHz). The first pulse width is adjusted to give a π pulse and the second pulse width is set for a 2π pulse. The calculated echo efficiency is ~18% in intensity, which is comparable to the experimental value in Fig. 3(b).

In Fig. 3(d), we increased laser power by a factor of ~2 and enlarged focused beam diameters by a factor of ~1.5. At high power, the laser was unstable so that data acquisition

time was shortened by increasing the probe scanning-step increment to 10 μs. Due to the discrete probe scanning and the unstable laser, the noise in the data is larger than in Fig. 3(b). The observed echo efficiency is very high $\sim$50% in intensity. However, the unexpected peaks at $\sim$30 μs after each pulse are still under investigation. The apparent narrower widths of FID and the echo signals in comparison with Fig. 3(b) are an artifact of the large discrete scanning step.

In Fig. 4, we theoretically analyze resonant Raman excited echoes in detail. In Fig. 4(a), the calculated echo efficiencies (defined as the ratio of echo to FID amplitude) are plotted as a function of the second Raman pulse area for a fixed first Raman pulse are of π. The three curves (dotted, solid, and dashed) correspond to three different optical homogeneous decay rates γ, as shown. These are chosen so that $\gamma \ll \Omega$, $\gamma \sim \Omega$, and $\gamma \gg \Omega$, respectively. The curves in Fig. 4(b) show echo efficiencies as a function of the first pulse area (second pulse area held fixed at 2π). The absolute echo amplitudes corresponding to Figs. 4(a) and 4(b) are shown in Figs. 4(c) and 4(d), respectively.

As seen in Fig. 4, the echo efficiency or amplitude strongly depends on the ratio of γ to Ω. In particular, Figs. 4(c) and 4(d) show that, when optical Rabi flopping is important (small γ), the echo amplitude oscillates with a period of 2π in the first pulse area [dotted curve in Fig. 4(d)] and 4π in the second pulse area [dotted curve in Fig. 4(c)]. This is as expected from the physical arguments given earlier. Note that the echo efficiency in Fig. 4(b) appears nearly independent of the first pulse area, even though the absolute echo amplitude varies considerably. In the case of large γ, the echo amplitude does not depend strongly on pulse area. This case is analogous to the CPT limit in that the excited atoms have dephased, but not yet decayed to the ground states. The fact that the echo efficiency is still close to 20% means that even low-power lasers should give easily observable echoes, and therefore be adequate for many applications.

In summary, we demonstrated efficient coherence excitation and rephasing using resonant Raman pulses in an optically dense rare-earth doped solid of Pr^{3+}:Y_2SiO_5. We also showed that the coherence rephasing is very efficient using the optical π-2π excitation scheme. By providing high echo efficiency without the need for atomic state preparation, high power laser, or long interaction time, this technique offers practical advantages in applications ranging from high resolution spectroscopy to high-density, high-speed optical memory.

We acknowledge discussions with Professor S. Ezekiel of the Massachusetts Institute of Technology. This study was supported by Air Force Research Laboratory (Grant No. F30602-96-2-0100), U.S. Air Force Office of Scientific Research (Grant No. F49620-96-1-0395), and National Science Foundation (Grant No. ECS 9421304).

[1] R. M. Shelby, C. S. Yannoni, and R. M. MacFarlane, Phys. Rev. Lett. **41**, 1739 (1978).

[2] J. Mlynek, N. C. Wong, R. G. DeVoe, E. S. Kintzer, and R. G. Brewer, Phys. Rev. Lett. **50**, 993 (1983).

[3] B. S. Ham, M. S. Shahriar, M. K. Kim, and P. R. Hemmer, Opt. Lett. **22**, 1849 (1997).

[4] J. R. Gardner, M. L. Marable, G. R. Welch, and J. E. Thomas, Phys. Rev. Lett. **22**, 3403 (1993).

[5] M. Kasevich and S. Chu, Phys. Rev. Lett. **67**, 181 (1991).

[6] C. Monroe, D. M. Meekhof, B. E. King, W. M. Itano, and D. J. Wineland, Phys. Rev. Lett. **25**, 4714 (1995).

[7] G. Alzetta, A. Gozzini, L. Moi, and G. Orriols, Nuovo Cimento B **36**, 5 (1976); H. R. Gray, R. M. Whitley, and C. R. Stroud, Jr., Opt. Lett. **3**, 218 (1978).

[8] J. Oreg, F. T. Hioe, and J. H. Eberly, Phys. Rev. A **29**, 690 (1984).

[9] R. M. Shelby, A. C. Tropper, R. T. Harley, and R. M. Macfarlane, Opt. Lett. **8**, 304 (1983); Y. Fukuda, M. Tanigawa, and T. Hashi, *ibid.* **8**, 301 (1983); M. Tanigawa, Y. Fukuda, M. Kunitomo, T. Hashi, and T. Mishina, J. Opt. Soc. Am. B **9**, 313 (1992).

[10] T. Blasberg and D. Suter, Phys. Rev. B **51**, 6309 (1995).

[11] S. E. Harris, Phys. Rev. Lett. **70**, 552 (1993).

[12] B. S. Ham, P. R. Hemmer, and M. S. Shahriar, Opt. Commun. **144**, 227 (1997).

[13] Y. Hukuda, K. Yamada, and T. Hashi, Opt. Commun. **44**, 297 (1983).

[14] E. C. Hoffmann, M. Hubrich, and A. Schweiger, J. Magn. Reson., Ser. A **117**, 16 (1995).

[15] R. W. Equall, R. L. Cone, and R. M. Macfarlane, Phys. Rev. B **52**, 3963 (1995).

[16] K. Holliday, M. Croci, E. Vauthey, and U. P. Wild, Phys. Rev. B **47**, 14 741 (1993).

[17] B. S. Ham, M. S. Shahriar, and P. R. Hemmer, Opt. Lett. **22**, 1138 (1997); S. E. Harris, J. E. Field, and A. Imamoglu, Phys. Rev. Lett. **64**, 1107 (1990).